AGU PUBLICATIONS

Geophysical Research Letters

RESEARCH LETTER
10.1002/2015GL067478

Key Points:
- Extreme precipitation in certain regions is associated with infrequently occurring synoptic patterns
- Storms impacting the Pacific Northwest are synoptically different than those impacting the Southwest
- SOMs are a valuable tool to relate the large-scale synoptic setting to local extreme precipitation

Supporting Information:
- Figures S1–S4 and Table S1

Correspondence to:
D. Swales,
dustin.swales@noaa.gov

Citation:
Swales, D., M. Alexander, and M. Hughes (2016), Examining moisture pathways and extreme precipitation in the U.S. Intermountain West using self-organizing maps, *Geophys. Res. Lett.*, *43*, 1727–1735, doi:10.1002/2015GL067478.

Received 28 DEC 2015
Accepted 25 JAN 2016
Accepted article online 26 JAN 2016
Published online 19 FEB 2016

Examining moisture pathways and extreme precipitation in the U.S. Intermountain West using self-organizing maps

Dustin Swales[1,2], Mike Alexander[2], and Mimi Hughes[1,2]

[1]Cooperative Institute for Research in Environmental Sciences, University of Colorado Boulder, Boulder, Colorado, USA, [2]NOAA/Earth System Research Laboratory, Boulder, Colorado, USA

Abstract Self-organizing maps (SOMs) were used to explore relationships between large-scale synoptic conditions, especially vertically integrated water vapor transport (IVT), and extreme precipitation events in the U.S. Intermountain West (IMW). By examining spatial patterns in the IVT, pathways are identified where moisture can penetrate into the IMW. A substantial number of extreme precipitation events in the IMW are associated with infrequently occurring synoptic patterns. The transition frequency between each of the SOM nodes, which indicate temporal relationships between the patterns, identified two synoptic settings associated with extreme precipitation in the IMW: (1) a landfalling, zonally propagating trough that results in a concentrated IVT band that moves southward as the system moves inland and (2) a southwesterly storm track associated with strong ridging over the coast that results in persistent IVT transport into the Pacific Northwest that can last for several days.

1. Introduction

During the cool season, the semiarid climate of the U.S. Intermountain West (IMW) often experiences extreme precipitation events associated with landfalling extratropical cyclones [*Leung and Qian*, 2009; *Neiman et al*., 2013; *Rutz and Steenburgh*, 2012; *Rutz et al*., 2014]. In the IMW, a majority of these extreme precipitation events are linked to atmospheric river (AR) events on the coast that penetrate into the interior of the western United States. [*Neiman et al*., 2013; *Rutz and Steenburgh*, 2012; *Rutz et al*., 2014]. An example of one such event was observed in January of 2010 when an AR event brought widespread precipitation, high-elevation blizzard conditions, flash flooding, and loss of life to the Southwest United States. [*Neiman et al*., 2013; *Hughes et al*., 2014].

Understanding how these systems transport moisture into the IMW and the pathways they take through the complex terrain is a relatively new area of study. The moisture pathways associated with storms originating over the Pacific may vary greatly between adjacent regions in the IMW. For example, moisture associated with extreme precipitation events in Northern Idaho passes through the Columbia River valley, whereas moisture that impacts Southern Idaho often passes over the California central valley and continues northeastward around the high Sierras [*Alexander et al*., 2015 and *Rutz et al*., 2015].

Over the past 15 years, the use of self-organizing maps (SOMs) [*Kohonen*, 2001] has expanded within a wide variety of disciplines [*Kaski et al*., 1998; *Oja et al*., 2003; *Liu and Weisberg*, 2011]. SOMs are a type of neural network algorithm that uses unsupervised learning to organize input data into representative groups, where neighboring patterns are more similar than distant patterns. SOMs, being a nonlinear method, have advantages over traditional linear methods such as principal component analysis (PCA). When using PCA, the number of components to retain is highly dependent on the ability to represent the system using orthogonal functions, which can be problematic in highly nonlinear systems. *Reusch et al*. [2005] compared the ability of SOMs to PCA on synthetic data sets and found that PCA is not able to isolate blended (nonlinear) patterns, while SOMs can.

In the geosciences, where data sets are consistently expanding and becoming more complex, SOMs have become a valuable tool for reducing data set dimensionality and organization. For example, *Johnson et al*. [2008] used SOMs to describe the eastward shift of the North Atlantic Oscillation (NAO) observed over the past 35 years, and *Nigro and Cassano* [2014] applied SOMs to identify surface wind patterns over the Ross Ice Shelf in Antarctica. SOMs have also been applied to help better understand extreme weather and climate events [*Cassano et al*., 2015, 2006; *Cavazos*, 2000]. *Cassano et al*. [2015] used SOMs to relate localized extreme temperature events in the Arctic to the large-scale synoptic environment. For a thorough review of the use of SOMs in the atmospheric and oceanic sciences, see *Liu and Weisberg* [2011].

The IVT is a useful quantity to study moisture transport; however, it is highly nonlinear, especially in areas with complex terrain. Using a method, such as SOMs, which is not constrained by orthogonality can be more useful than traditional linear methods. In this study we use SOMs of IVT to explore the relationship between the large-scale synoptic environment and extreme precipitation events in the IMW.

2. Data and Methods

2.1. CFSR Data Set

The Climate Forecast System Reanalysis (CFSR) data set provided by the National Center for Environmental Prediction is the main source for the gridded atmospheric fields used in this study [*Saha et al*., 2010]. The CFSR is a global atmospheric, oceanic, land, and sea ice reanalysis, with horizontal resolution of T382 (~40 km) and 64 vertical levels. The CFSR analysis fields are archived on 0.5° horizontal grid with a temporal resolution of 6 h. For this study we focus on the cool-season months (October–March) from 1979 to 2010 and our domain extends from 130°W to 110°W and 30° to 50°N.

2.2. Livneh Precipitation Data Set

High-resolution (1/16°) precipitation data recently developed by *Livneh et al*. [2013, hereafter L2013] were used to identify days with high amounts of precipitation. The data set covers the conterminous United States and extends into southwestern Canada to cover the Columbia River watershed. This data set is daily and derived from nearly 20,000 NOAA Cooperative Observer stations. The temporal and spatial domain is identical to that of the CFSR data set mentioned above.

2.3. Hierarchical SOMs of Standardized IVT Anomaly

For all of the cool-season days, the SOM analysis is performed on the magnitude of the standardized integrated vapor transport anomaly, |IVT|′, using only CFSR grid points over land. The IVT is computed using the horizontal CFSR winds $\overline{V}$ and specific humidity q on model pressure levels from the surface to 300 hPa ($\mathrm{IVT} \equiv \int_{\mathrm{SFC}}^{300\mathrm{hPa}} \left(\overline{V}q/g\right)\mathrm{d}p$) [e.g., *Neiman et al*., 2008]. The IVT in the Pacific maritime environment and the coastal western United States is generally much greater than in the IMW; so in order to highlight the IVT anomalies over the IMW we trained the SOMS only using land points and standardized the anomalies by dividing the grid values by the local standard deviation for each month.

The SOM patterns are obtained from the composite average of the days within each node, where the number of patterns is chosen by the user prior to training the SOM. In this study, we use two sets of SOMs. First, we construct a low order 2×2 SOM of |IVT|′. The most frequently occurring pattern, which occurs on nearly half of the days (Figure 1), is negative over most of the domain, and little precipitation occurs over the western United States on the days in this "dry node" (supporting information Figure 1). We then remove these days with negative |IVT|′ and negative precipitation anomalies and train our SOM on the remaining days but using a 3×3 SOM. Prior to settling on this SOM architecture, we explored using a wide variety of SOM node configurations and parameters (i.e. learning rate, neighborhood function, and radius). In all cases, the dominant patterns were nearly identical, suggesting these results are not sensitive to the SOM configuration chosen.

2.4. Extreme Precipitation Mapping

To relate the SOM patterns to extreme events, we identify extreme precipitation days in L2013 at every grid point throughout the domain. We define extreme as the top 2% of days with any precipitation that occurred during the cool season (October–March) during the 32 years of the study. We then map the days at each point in this extreme precipitation climatology to the days in each SOM node. This provides us with a map relating each SOM node to extreme precipitation throughout the IMW.

2.5. SOM Transitions

With any clustering technique, computing the transition frequency from each node (or centroid) to the other nodes can provide valuable information on how the nodes temporally relate to each other. Since the SOM composites are made up of individual days, we can simply look at all of the days in each node and see which node they occurred at some other time. Here we compute the 1 day lead transition frequency for all nine nodes in the 3×3 SOM; in this case, in addition to node-node transitions, transitions can leave the SOM because of the dry-day removal.

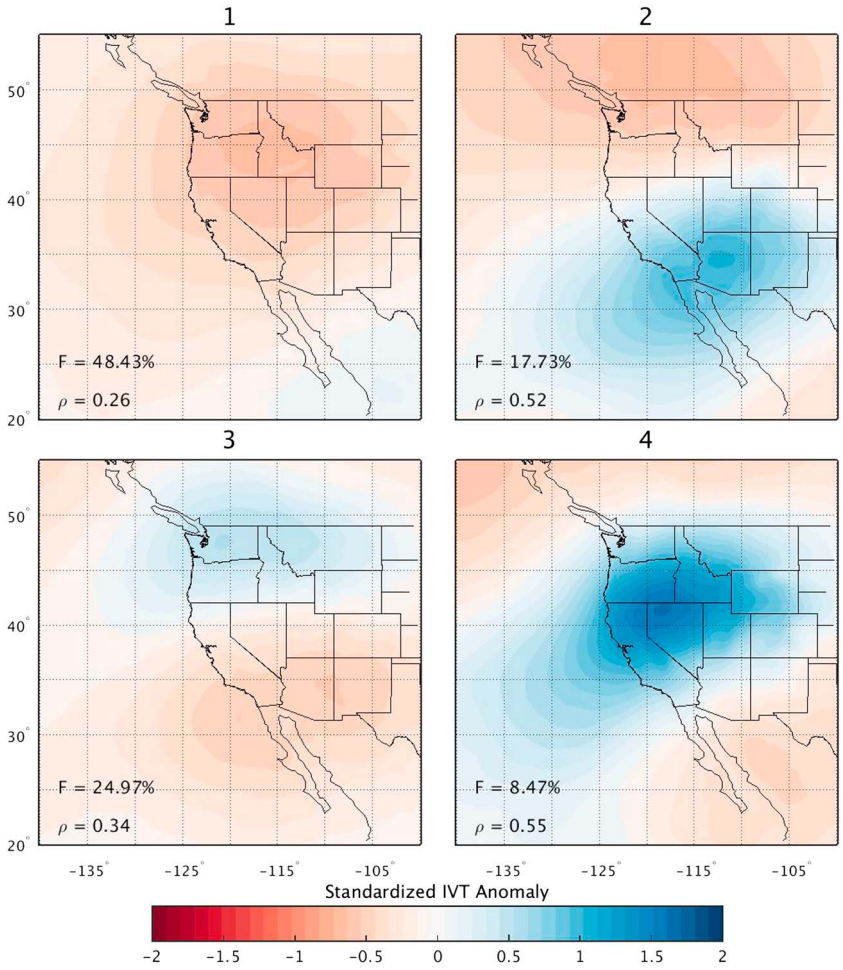

Figure 1. A 2 × 2 SOM composite of standardized integrated vapor transport anomaly. In the lower left corner of each plot, the frequency of occurrence for each pattern (F) and the mean pattern correlation (ρ) are labeled.

3. Results

3.1. SOMs and SOM Pattern Transitions

In order to capture the large-scale synoptic setting, composites of the synoptic IVT and 500 hPa geopotential height fields were generated over a larger domain. Figure 1 reveals four distinctive |IVT|′ patterns: predominantly dry (1), southern (2), northern (3), and central (4). Within each of these patterns, there appears to be little or no seasonal dependence (supporting information Figure 2). The dry pattern is the most frequently occurring pattern (~48% of the time) and has a low mean pattern correlation (0.26). Creating composites of similar patterns with slightly different anomaly locations can result in a "broadening" or "smearing" of the anomaly in the composites. Examining the mean pattern correlation can help us determine if this is true. The mean pattern correlation indicates how well the patterns on individual days assigned to a SOM node resemble the composite average of all days within that node. Given the low mean pattern correlation in the dry pattern, we further examined the ratio of |IVT|′ and the standard deviation of |IVT|′ (supporting information Figure 3). This can be thought of as signal-to-variability map, and when used in conjunction with the anomaly map (Figure 1), we can determine if the anomalies are statistically significant. In both Figure 1 and supporting information Figure 1, the signs and locations of the maximum and minimum for the dry pattern are the same (spatial correlations $>$0.98), but the magnitude is much greater in supporting information Figure 1, which suggests lower variability where the signal is strongest, in this case over the IMW.

The 2 × 2 SOM is useful for identifying the days with little to no observed widespread precipitation over the IMW but does not provide enough detail to resolve the wide variety of systems that are responsible for days with

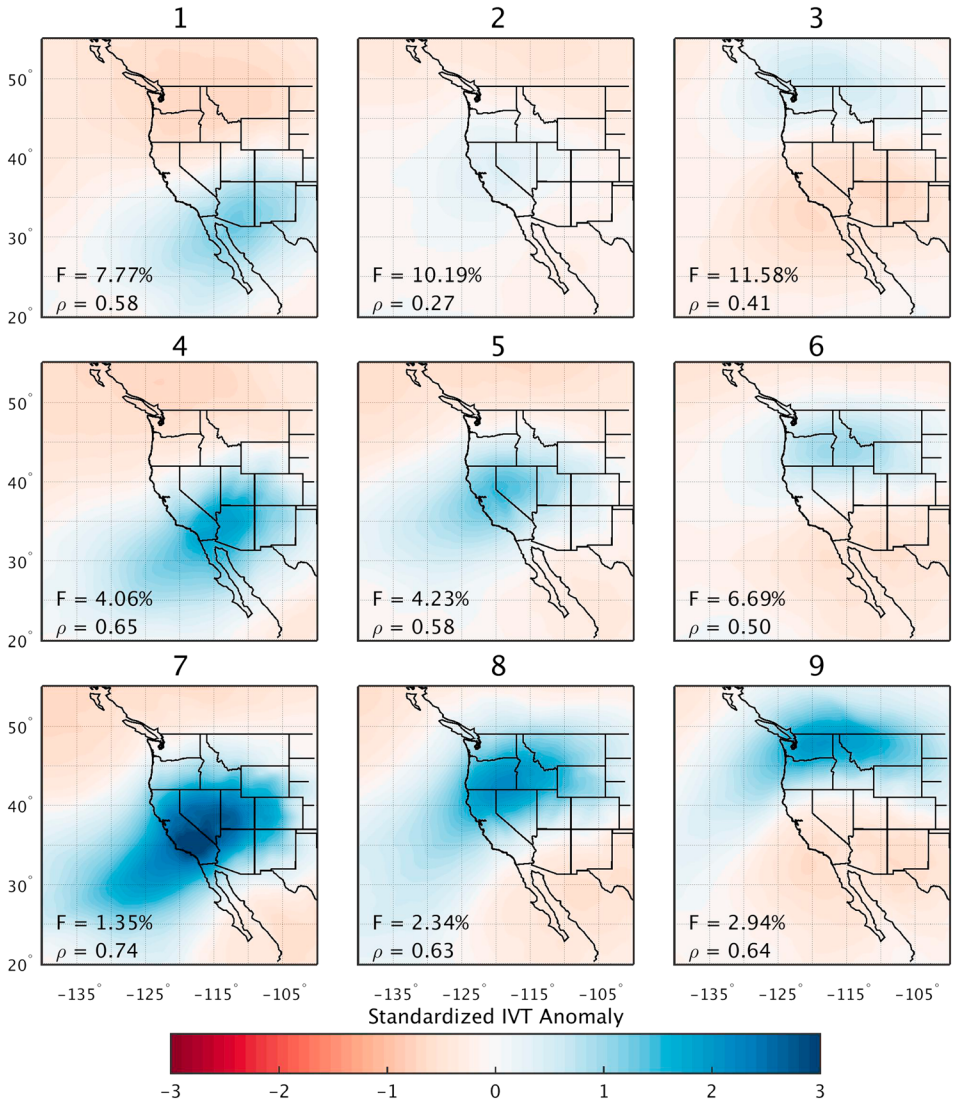

Figure 2. A 3 × 3 SOM composite of standardized integrated vapor transport anomaly, |IVT|'.

precipitation. To do this, we train a 3 × 3 SOM on the 52% of "wet" days remaining after dry-day removal. For the 3 × 3 configuration, composites were generated for |IVT|' (Figure 2) and IVT with 500 hPa geopotential height contours overlaid (Figure 3). The primary patterns, typically centered about the corner patterns, in the 3 × 3 |IVT|' composite are southern (1), central (7), and northern (3, 6, and 9). For the northern patterns, we refer to these three patterns as one because of their large cross-pattern correlations (~0.9; supporting information Table 1). The northern patterns occur much more frequently than the other primary patterns, ~21% of days, whereas the southern and central patterns account for only ~8 and ~1.5% of days, respectively. These frequencies are consistent with previous studies of ARs in the western United States [*Neiman et al.*, 2008; *Rutz et al.*, 2015]. There are relatively little to no seasonal dependencies observed within the nodes (supporting information Figure 4), with the exception being the northern central pattern, which shows a middle-to-late season bias.

Transitional patterns are identified by examining the cross-pattern correlations (supporting information Table 1). Off-corner patterns that correlate similarly with a pair of neighboring primary patterns are defined as transitional. These patterns generally show a smooth transition between the primary patterns and are identified as southern central (4), northern central (8), and hybrid central (5). The southern central pattern is associated with a trough centered over northern California, forcing moisture to the south and around the high Sierra Nevada into southern California and Nevada. Hybrid central has characteristics common to

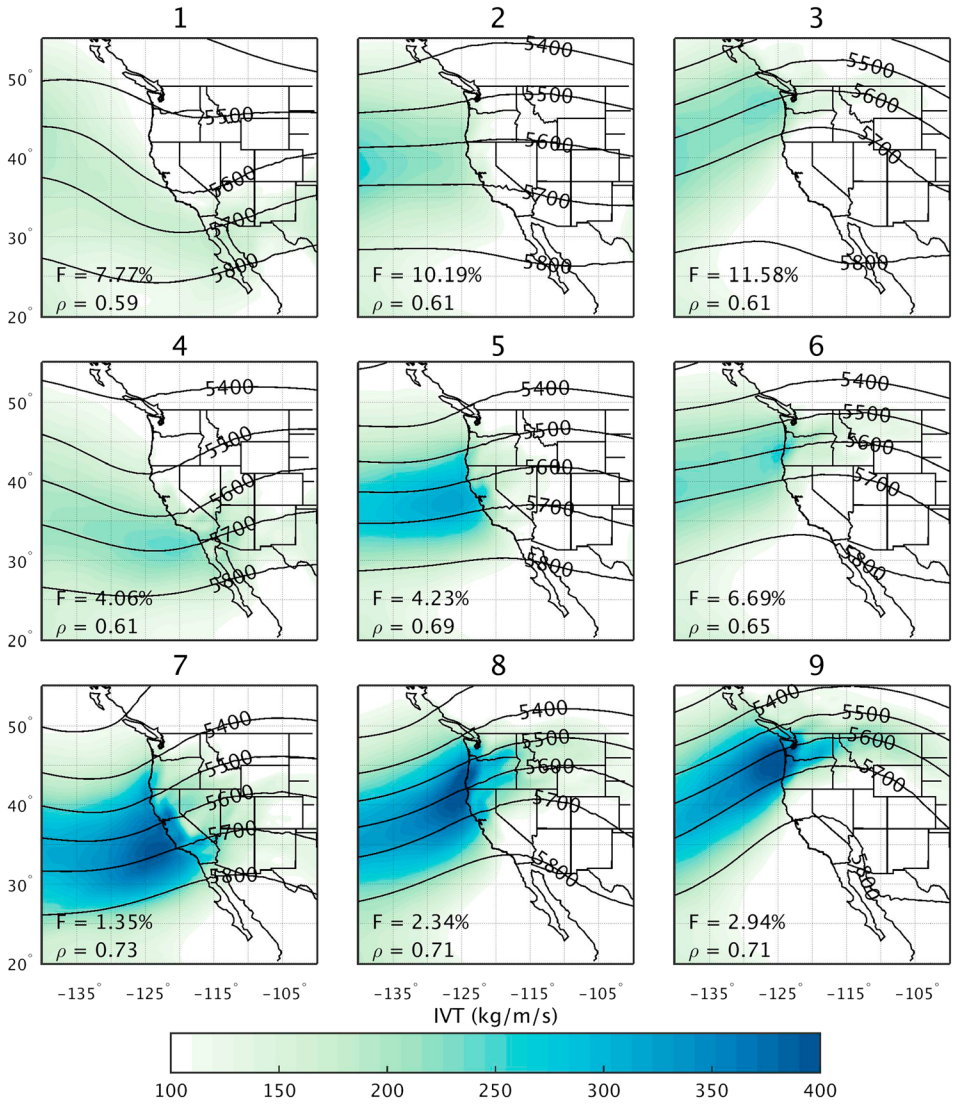

Figure 3. A 3 × 3 SOM composite of integrated vapor transport, IVT. Overlaid on the IVT contours are contours of the 500 hPa geopotential height (m).

all of the primary patterns and can be thought of as a weighted average of all the days used in the SOM. The northern central pattern is associated with a moderate strength ridge centered over the Southwest United States. (Figure 3), leading to a more southwesterly storm track. Pattern (2) is neither a primary nor transitional pattern but rather consists of storm systems that are offshore and have yet to make landfall (Figure 3). Since we train our SOM using points over land only, storm systems responsible for some precipitation but that are mostly located offshore and have a weak |IVT|′ signal over land, generally get grouped together in this pattern. The 500 hPa geopotential height for pattern (2) shows a nearly zonal pattern resulting from compositing systems with differing positions offshore.

We examine how each node relates to each other temporally by computing the node transition frequency. To compute the transition frequency for any particular node, all of the days in that node are examined and we determine which of the other nodes contain the day after (lag). Performing this for all of the days in all of the nodes gives us a table of how the patterns transition to one another or to the dry pattern identified in the 2 × 2 SOM (Table 1).

From a synoptic viewpoint, we expect there to be transitioning between some of the nodes. For example, in an extratropical cyclone, moisture-rich air often extends from ahead of the cold front southwesterly away

Table 1. One Day Lead Transitional Frequencies Between the 3 × 3 SOM Node Configurations[a]

1			2			3		
21.32	9.90	3.08	11.56	**19.10**	7.83	1.77	11.06	**33.19**
7.91	2.20	1.32	6.20	9.72	9.88	0.29	1.62	12.68
0.22	0.22	0.22	1.17	2.85	3.52	0.15	1.77	5.90
53.63			28.14			31.56		
4			5			6		
33.20	7.56	1.68	11.70	14.52	1.21	3.06	15.05	9.44
21.43	4.62	0.42	15.73	**19.35**	5.24	1.79	6.38	**22.96**
4.62	0.84	0.00	8.87	8.87	3.63	1.02	5.61	6.89
25.63			10.88			27.81		
7			8			9		
21.52	6.33	1.27	3.65	13.87	0.73	1.16	6.98	19.77
32.91	6.33	2.53	5.84	18.25	17.52	0.00	1.75	25.00
24.05	2.53	1.27	8.76	**20.44**	6.57	0.00	9.88	**24.42**
1.27			4.38			11.05		

[a]The number below each box represents the 1 day lead transition frequency from the dry days removed using the 2 × 2 SOM.

from the surface low. Thus, when these systems move zonally over the coast, the location of the moisture-rich air is often southwest of the surface low. Examination of the evolution of the IVT field of a landfalling extratropical cyclone would reveal a band of moisture moving down the coast.

Examining the lag transitions for the dominant central pattern, we notice that ~54% of the time this central pattern transitions into more southern nodes, southern, and southern central, consistent with an extratropical cyclone making landfall and the cold front sweeping south down the coast. However, this is not true for the dominant northern patterns. Northern patterns transition to more southerly patterns (i.e., northern central and central) only ~10% of the time and instead often last several days (i.e., northern patterns exhibit persistence). Treating the three northern patterns as one and recomputing the transition frequency we observe that ~50% of the time the northern pattern is persistent for at least 2 days, whereas the southern and central patterns persist about 20–25% of the time.

This persistence suggests that the synoptic conditions associated with these northern patterns are different than that those of southern patterns. One possible explanation for this persistent northern pattern would be

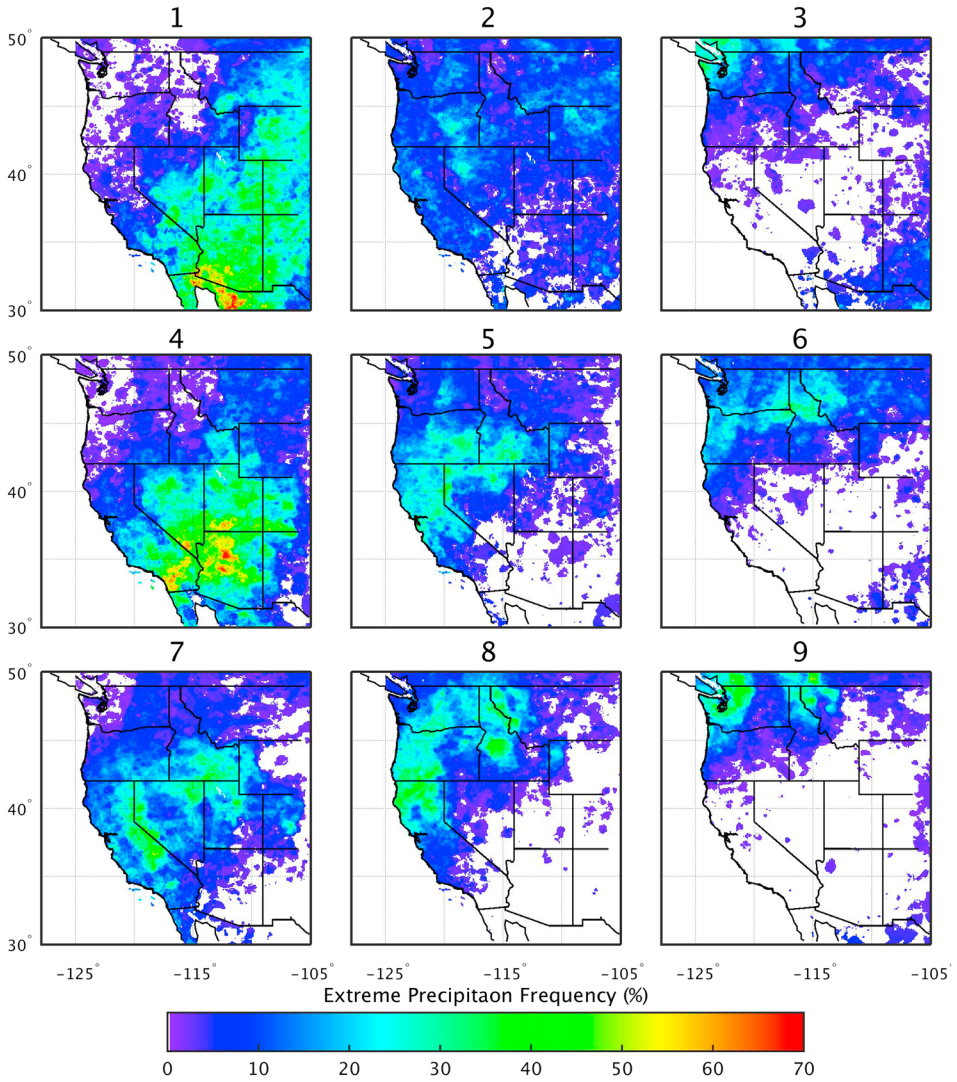

Figure 4. Extreme precipitation frequency derived from high-resolution precipitation data set (L2013) mapped onto 3 × 3 SOM nodes.

a southwest to northeast storm track, which would result in a persistent IVT anomaly across the coast for several days, whereas a west to east storm track would produce an IVT anomaly that moves southerly. During the cool season in the Pacific Northwest, a southwesterly storm track is often observed in combination with storms moving over the Gulf of Alaska [*Rodionov et al.*, 2007]. In this study our domain does not extend far enough to the north and west to capture systems in the Gulf of Alaska; however, ridging over the western United States often accompanies these systems, which we can capture within our domain. Examining the 500 hPa geopotential height fields (Figure 3), it is evident that the central to southern progression is associated with a trough propagating zonally, while the persistent northern pattern is associated with a stationary ridge over the coast.

3.2. Extreme Mapping

To examine how each of the 3 × 3 SOM nodes relates to extreme precipitation events in the IMW, we mapped the days from each node to L2013 extreme precipitation days (Figure 4). Comparing the |IVT|′ patterns and the extreme mapping illustrates how minor differences in the location of the |IVT|′ maximum can strongly affect extreme precipitation event distribution across the western US.

The southern pattern, which accounts for 7.7% of the days with precipitation, corresponds with roughly 40–50% of the extreme events that occur throughout the Southwest United States and upward of 65% of

the extreme events in some parts of southern Arizona. Also, this southern pattern appears to be contributing up to ~40% of extreme precipitation events deep into the IMW, in places such as Utah, Colorado, and Wyoming. The SOM southern central transitional pattern accounts for a majority of the remaining extreme events observed in the Southwest United States. Over the southern edge of the Colorado plateau, this pattern accounts for over 70% of extreme precipitation events at some locations. The northward shift of the |IVT|′ maximum from southern to southern central shows more extreme precipitation over the Mogollon Rim and less precipitation downstream in Colorado, Wyoming, and Montana, which suggests that the more southern pathway is less impeded by the high topography of the Mogollon Rim (southern terminus of the Colorado plateau) and can transport moisture further inland.

The central |IVT|′ pattern occurs less frequently than any other pattern, ~1.3% of the time, but at some locations in the Sierras and southern Idaho, this pattern is associated with upward of 40% of the extreme precipitation events. The spatial distribution of these extreme events also supports findings in a previous study where the pathways for the moisture associated with extreme precipitation events in southern Idaho were seen to take a path north through the California Central Valley before turning east toward southern Idaho [*Alexander et al*., 2015]. This pattern impacts the coastal mountains of Central and Northern California and penetrates into the IMW where it impacts southern and central Idaho.

Extreme precipitation along the western United States coast from Oregon into southern British Columbia is generally associated with the northern patterns. In the IMW these patterns are associated with extreme precipitation events in northern Idaho and western Montana. In the northern pattern, high IVT is confined to just west of the Cascade Mountains with a filament of high IVT air extending east through the Columbia River Valley, especially pattern 6 (Figure 2). Previous work by *Alexander et al*. [2015] and *Rutz et al*. [2015] both identify this preferred pathway for moisture through the Columbia River Valley and fuel storms downstream in northern Idaho and Western Montana.

4. Conclusions

We showed that using self-organizing maps (SOMs), trained on the magnitude integrated water vapor transport anomaly over the IMW, could be a valuable tool when trying to relate localized extreme precipitation to the large-scale synoptic conditions. In some regions of the IMW, a substantial amount (~70%) of the localized extreme precipitation is associated with infrequently (~1.5%) occurring synoptic conditions. SOMs first organize the data by using spatial patterns in the data and looking at the 1 day lag transition between the nodes further elucidates temporal relationships. We were able to identify two synoptic settings for storms impacting the western United States: (1) a landfalling, zonally propagating trough that results in a moisture band moving southward down the West Coast and (2) a stationary ridge pattern over the West Coast, causing persistent conditions that can last several days. Examining the SOM composites of IVT also identified preferred moisture pathways through the complex and high terrain. For example, moisture reaching central Idaho takes a path through the California Central Valley before turning northeastward, whereas moisture reaching northern Idaho and western Montana travels through the Columbia River Valley. These different pathways for northern and southern Idaho are identical to pathways identified by *Rutz et al*. [2015].

Acknowledgments
The authors would like to thank the Bureau of Reclamation for their financial support for this work and in particular Kathleen Holman for her feedback and constructive comments along the way, Nathaniel Johnson at GFDL for providing guidance in the early stages of this work, and also James Scott and Kelly Mahoney at the University of Colorado/CIRES for their helpful suggestions.

References

Alexander, M. A., J. D. Scott, D. Swales, M. Hughes, K. Mahoney and C. A. Smith (2015), Moisture pathways into the U.S. intermountain west associated with heavy winter precipitation events, *J. Hydrometeorol.*, doi:10.1175/JHM-D-14-0139.1, in press.

Cassano, E. N., A. H. Lynch, J. J. Cassano, and M. R. Koslow (2006), Classification of synoptic patterns in the western Arctic associated with extreme events at Barrow, Alaska, USA, *Climate Res.*, *30*, 83–97.

Cassano, E. N., J. M. Glisan, J. J. Cassano, W. J. Gutowski Jr., and M. W. Seefeldt (2015), Self-organizing map analysis of widespread temperature extremes in Alaska and Canada, *Climate Res.*, *62*, 199–218.

Cavazos, T. (2000), Using self-organizing maps to investigate extreme climate events: An application to wintertime precipitation in the Balkans, *J. Clim.*, *13*, 1718–1732.

Hughes, M., K. M. Mahoney, P. J. Neiman, B. J. Moore, M. Alexander, and F. M. Ralph (2014), The landfall and inland penetration of a flood-producing atmospheric river in Arizona. Part II: sensitivity of modeled precipitation to terrain height and atmospheric river orientation, *J. Hydrometeorol.*, *15*, 1954–1974.

Johnson, C. J., S. B. Feldstein, and B. Tremblay (2008), The continuum of Northern Hemisphere teleconnection patterns and a description of the NAO shift with the use of self-organizing maps, *J. Clim.*, *21*, 6354–6371.

Kaski, S. J., J. Kangas, and T. Kohonen (1998), Bibliography of self-organizing Map (SOM) papers: 1981–1997, *Neural Comput. Surv.*, *1*, 102–350.

Kohonen, T. (2001), *Self-Organizing Maps*, *Springer Series in Informational Sciences*, vol. 30, Springer.

Leung, L. R., and Y. Qian (2009), Atmospheric rivers induced heavy precipitation and flooding in the western U.S. simulated by the WRF regional climate model, *Geophys. Res. Lett.*, *36*, L03820, doi:10.1029/2008GL036445.

Liu, Y., and R. H. Weisberg (2011), A review of self-organizing map applications in meteorology and oceanography, self organizing maps—Applications and novel algorithm design, Dr. Josphat Igadwa Mwasiagi.

Livneh, B., E. A. Rosenberg, C. Lin, B. Nijssen, V. Mishra, K. M. Andreadis, E. P. Maurer, and D. P. Lettenmaier (2013), A long-term hydrologically based dataset of land surface fluxes and states for the conterminous United States: Update and extensions, *J. Clim.*, *26*, 9384–9392.

Neiman, P. J., F. M. Ralph, G. A. Wick, J. D. Lundquist, and M. D. Dettinger (2008), Meteorological characteristics and overland precipitation impacts of atmospheric rivers affecting the west coast of North America based on eight years of SSM/I satellite observations, *J. Hydrometeorol.*, *9*, 22–47.

Neiman, P. J., B. J. Moore, M. Hughes, K. M. Mahoney, J. M. Cordeira, and M. D. Dettinger (2013), The landfall and inland penetration of a flood-producing atmospheric river in Arizona. Part 1: Observed synoptic-scale, orographic and hydrometeorological characteristics, *J. Hydrometeorol.*, *14*, 460–484.

Nigro, A. M., and J. J. Cassano (2014), Identification of surface wind patterns over the Ross Ice Shelf, Antarctica, using self organizing maps, *Mon. Weather Rev.*, *142*, 2361–2378.

Oja, M., S. Kaski, and T. Kohonen (2003), Bibliography of self-organizing map (SOM) papers: 1998–2001 addendum, *Neural Comput. Surv.*, *3*, 1–156.

Reusch, D. B., R. B. Alley, and B. C. Hewiston (2005), Relative performance of self-organizing maps and principal component analysis in pattern extraction from synthetic climatological data, *Polar Geogr.*, *29*, 188–212.

Rodionov, S. N., N. A. Bond, and J. E. Overland (2007), The Aleutian Low, storm tracks, and winter climate variability in the Bering Sea, *Deep Sea Res., Part II*, *54*, 2560–2577.

Rutz, J. J., and W. J. Steenburgh (2012), Quantifying the role of atmospheric rivers in the interior western United States, *Atmos. Sci. Lett.*, *13*, 257–261.

Rutz, J. J., W. J. Steenburgh, and F. M. Ralph (2014), Climatological characteristics of atmospheric rivers and their inland penetration over the western United States, *Mon. Weather Rev.*, *142*, 905–921.

Rutz, J. J., W. J. Steenburgh, and F. M. Ralph (2015), The inland penetration of atmospheric rivers over Western North America, *Mon. Weather Rev.*, *143*, 1924–1944.

Saha, S., et al. (2010), The NCEP Climate Forecast System Reanalysis, *Bull. Am. Meteorol. Soc.*, *91*, 1015–1057.